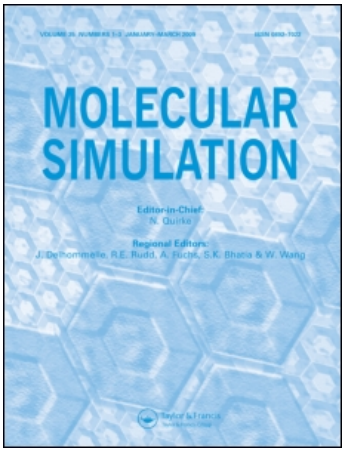

Molecular Simulation
Publication details, including instructions for authors and subscription information:
http://www.informaworld.com/smpp/title~content=t713644482

Combined Diffusive and Viscous Transport of Methane in a Carbon Slit Pore

Karl P. Travis[ab]; Keith E. Gubbins[a]
[a] Department of Chemical Engineering, Riddick Labs, North Carolina State University, Raleigh, NC, USA [b] Department of Chemistry, Imperial College, London

To cite this Article Travis, Karl P. and Gubbins, Keith E.(2000) 'Combined Diffusive and Viscous Transport of Methane in a Carbon Slit Pore', Molecular Simulation, 25: 3, 209 — 227
To link to this Article: DOI: 10.1080/08927020008044126
URL: http://dx.doi.org/10.1080/08927020008044126

Molecular Simulation, 2000, Vol. 25, pp. 209–227
Reprints available directly from the publisher
Photocopying permitted by license only

COMBINED DIFFUSIVE AND VISCOUS TRANSPORT OF METHANE IN A CARBON SLIT PORE

KARL P. TRAVIS* and KEITH E. GUBBINS†

Department of Chemical Engineering, Riddick Labs, North Carolina State University, Raleigh, NC 27695-7905, USA

(Received April 1999; accepted June 1999)

The transport of mass through porous materials can occur by essentially two different mechanisms: (1) diffusion and (2) viscous flow. The former occurs when there is a gradient in chemical potential of the pore fluid, while the latter occurs in the presence of a pressure gradient. In general, fluid transport occurs by both of these mechanisms and their respective contributions to the total intra-pore flux are approximately additive. Experimentally, there is no unambiguous way of determining the individual contributions to the total flux of these two modes of transport. Fortunately, molecular simulations does provide a solution.

We present a novel simulation method in which the separate contributions to the total flux are determined. The method involves the use of two non-equilibrium molecular dynamics techniques: dual control volume grand canonical molecular dynamics (DCV GCMD) and an algorithm for simulating planar Poiseuille flow. We apply this technique to study the combined (viscous and diffusive) transport of methane through single slit-shaped graphite pores of width 2.5, 5.0 and 10.0 methane diameters. We find that the viscous contribution to the total intra-pore flux through each of these pores is 10%, 15% and 34%, respectively.

Keywords: Transport diffusion; viscosity; Poiseuille flow; non-equilibrium molecular dynamics

1. INTRODUCTION

The development of the technique of Dual Control Volume Grand Canonical Molecular Dynamics (DCV GCMD) [1–3] has enabled the phenomenon of transport diffusion to be simulated directly, with conditions close to those in a real diffusion experiment, in which gradients in the

*Present address: Department of Chemistry, Imperial College, London SW7 2AY.
†Corresponding author.

chemical potential drive the flow and pressure gradients can be present. In the DCV GCMD technique, a gradient in chemical potential is established by placing two particle reservoirs at either end of a single pore and maintaining them at fixed, but different, chemical potentials. This method has been used to study the transport diffusion of methane in graphite [3], diffusion of various gases in zeolite frameworks [4], diffusion through polymer membranes [5], and diffusion of a mixture of oxygen and nitrogen through a graphite slit-pore [6–8]. One drawback of DCV GCMD simulations is that one calculates only an effective transport diffusivity, which is not a true diffusion coefficient since it contains a contribution due to viscous flow. An ability to calculate the viscous contribution to the total flow is important in itself, but it is also desirable from the point of view of obtaining the transport diffusivity. To date, the only suitable method of achieving this has involved an indirect calculation involving equilibrium molecular dynamics [9]. However, the equilibrium approach is statistically inefficient. In this paper we present a novel scheme for calculating the viscous contribution to the flow directly *via* non-equilibrium molecular dynamics and show how it can be used to decompose the effective transport diffusivity into its more fundamental and useful components.

2. TRANSPORT THEORY

For a single component fluid flowing through a slit pore (in which the solid membrane particles are effectively stationary) under isothermal conditions, the treatment of Mason and co-workers [10, 11] leads to the following expression for the total molar flux of the fluid in the laboratory frame [12]

$$J_x^{\text{tot}} = -L_f \frac{d\mu}{dx} - \frac{\rho H^2}{12\eta} \frac{dp}{dx}, \tag{1}$$

where the flow is in the x-direction, the coefficient L_f is a linear phenomenological transport coefficient arising from diffusion flow, $(d\mu/dx)$ is the gradient in fluid chemical potential, ρ is the molar fluid density (concentration), η is the fluid viscosity and p is the hydrostatic pressure. The second term on the right side of Eq. (1) represents the viscous contribution to the total flux while the first term represents the diffusive contribution, *i.e.*, $J_x^{\text{tot}} = J_x^D + J_x^V$.

Two assumptions were made in the derivation of the viscous flux term, J_x^V, arising in Eq. (1). The first assumption is that the Navier-Stokes equations

are valid for the length scale of interest. Solving these equations for the case of planar Poiseuille flow at low Reynolds number yields the streaming velocity u_x. The second assumption is that the density of the system is uniform. Integrating the product ρu_x over the z coordinate yields J_x^V. For narrow pores, both assumptions can be expected to be invalid [13].

The diffusive flux is generally written in terms of a mobility coefficient (also referred to as the corrected diffusivity), D_0, where D_0 is defined as $D_0 \equiv L_f (k_B T/\rho)$, giving

$$J_x^D = -\frac{\rho D_0}{k_B T}\frac{d\mu}{dx} \tag{2}$$

This expression can also be recast into the more familiar Fickian form:

$$J_x^D = -D_0\left(\frac{d\ln f}{d\ln \rho}\right)\frac{d\rho}{dx} = -D_t\frac{d\rho}{dx} \tag{3}$$

where f is the fugacity of the bulk external gas phase in equilibrium with the pore fluid. The term $(d\ln f/d\ln \rho)$ is often referred to as the Darken factor. The product $D_0(d\ln f/d\ln \rho)$ is then called the transport diffusivity, D_t.

Using the Gibbs-Duhem relation, the gradient term (dp/dx) can be expressed in terms of a gradient in the fluid density. The expression for the total flux then becomes

$$J_x^{\text{tot}} = -\left[D_0 + \frac{\rho k_B T H^2}{12\eta}\right]\left(\frac{d\ln f}{d\ln \rho}\right)\left(\frac{d\rho}{dx}\right) \tag{4}$$

where the quantity in square brackets multiplied by the Darken factor is an effective diffusivity,

$$J_x^{\text{tot}} = -D_t^{\text{eff}}\frac{d\rho}{dx} \tag{5}$$

It is this quantity, D_t^{eff}, which is calculated in DCV GCMD simulations involving pressure gradients. However, it is desirable to calculate D_t rather than D_t^{eff} from a theoretical point of view, and to enable comparisons to be made with experimental diffusion coefficients, which are measured under isobaric conditions. The mobility coefficient, D_0, is a more fundamental quantity than D_t^{eff}, since it is directly related to equilibrium fluctuations in the barycentric velocity of the fluid. The mobility coefficient can be further decomposed into the sum of a self diffusivity, D_S, and a diffusivity that is

related to the correlations between the momenta of different molecules, D_ξ [12]

$$D_0 = D_S + D_\xi \tag{6}$$

The cross correlation term will become negligible as ideal gas behaviour is approached. In narrow pores where the adsorbate concentration can be high, the role played by D_ξ in transport mechanisms can be expected to be significant. A decomposition of the effective transport diffusivity is therefore essential in studies of diffusion-limited separation processes in confined systems.

3. SUBTRACTION METHOD

The transport diffusivity can be calculated directly from the product of the mobility coefficient and the Darken factor, both of which can be obtained from equilibrium simulations. However in practice, the correlation function $\langle \mathbf{u}(t) \cdot \mathbf{u}(0) \rangle$ has a long time tail, which means that the integral converges very slowly. The equilibrium route to D_0 is thus an extremely inefficient one.

The use of non-equilibrium molecular dynamics offers an efficient, alternate route to the transport diffusivity. Instead of calculating D_0 directly from equilibrium simulations, the viscous contribution to the flux in the combined transport simulations is calculated directly. The transport diffusivity is then obtained from the ratio of the diffusive part of the total flux to the concentration gradient. This is the essence of our viscous subtraction method (VSM). The recipe for carrying out VSM can be summarised as follows:

(1) Conduct a DCV GCMD simulation at a fixed temperature and activity gradient. Calculate the total intra-pore flux and the mean density.
(2) Perform a planar Poiseuille flow simulation at the same pressure gradient as used in the DCV GCMD simulation and at the same mean density and temperature. Calculate the mean viscous flux by numerically integrating the flux profile.
(3) Subtract the viscous flux obtained in (2) from the total flux obtained in (1) and calculate the transport diffusivity from the ratio of the resulting flux to the concentration gradient from (1).

The important step is (2). The Poiseuille flow simulations are conducted in such a way that only viscous flow may occur. This is achieved by applying a

constant force in the flow direction to each particle in the system. This fact, coupled with the use of periodic boundaries in the unconfined directions, ensures that the fluid remains homogeneous in the flow direction (no density gradients). Whilst this method of performing planar Poiseuille flow has been described previously [13, 14], its application in decomposing the total flux for combined transport is new. If the mobility coefficient is required, it can be determined indirectly using Eq. (3) together with the Darken factor which is easily obtained from equilibrium Monte Carlo simulations. Once the mobility has been calculated, the cross coupling diffusivity can then be calculated by subtracting from it the coefficient of self diffusivity. This latter quantity, unlike D_0, is easily calculated from equilibrium molecular dynamics simulations since it is a single particle property.

In the remainder of this paper we present results for methane transport through a carbon slit pore at 3 different pore widths: $H = 2.5\,\sigma_f$, $H = 5.0\,\sigma_f$ and $H = 10.0\,\sigma_f$, (σ_f being the methane Lennard-Jones diameter, $\sigma_f = 0.381$ nm). This system has been studied before [3, 9], though only for $H = 2.5\,\sigma_f$.

4. SIMULATION DETAILS

4.1. Model Description

We represent the interaction of the methane molecules with the graphite planes in our model by a smooth 10-4-3 potential due to Steele [15]. This potential is a function of the z-coordinate only. To represent opposing graphite planes in a slit-pore we employ a superposition of two potential functions

$$\Phi_{sf} = 4\pi\varepsilon_{sf}\sigma_{sf}^2\Delta n_c\left[\frac{1}{5}\left(\frac{\sigma_{sf}}{(H/2)-z}\right)^{10} - \frac{1}{2}\left(\frac{\sigma_{sf}}{(H/2)-z}\right)^{4} - \frac{\sigma_{sf}^4}{6\Delta((H/2)-z+0.61\Delta)^3} + \frac{1}{5}\left(\frac{\sigma_{sf}}{(H/2)+z}\right)^{10} - \frac{1}{2}\left(\frac{\sigma_{sf}}{(H/2)+z}\right)^{4} - \frac{\sigma_{sf}^4}{6\Delta((H/2)+z+0.61\Delta)^3}\right] \quad (7)$$

where Δ is the inner layer spacing in graphite, which is taken to be 0.335 nm, $n_c = 114\,\text{nm}^{-3}$ is the carbon atom number density in graphite, H is the pore

width, defined as the distance between the centers-of-mass of the innermost graphite planes, while ε_{sf} and σ_{sf} are the Lennard-Jones parameters appropriate for interactions between a methane molecule and a carbon atom.

Methane is modeled as a single site Lennard-Jones particle. Interactions between methane molecules are spherically truncated (but not shifted). The truncation radius is taken to be $5\sigma_f$. We do not truncate the Steele 10-4-3 potential. Methane Lennard-Jones parameters are taken to be: $\sigma_f = 0.381$ nm, $\varepsilon_f/k_B = 148.1$ K, while the solid-fluid parameters are $\sigma_{sf} = 0.3605$ nm, $\varepsilon_{sf} = 64.4$ K.

We define our coordinate system such that the flow is in the x-direction and the graphite planes are separated along the z-direction.

4.2. DCV GCMD Algorithm

In the DCV GCMD algorithm, control volumes are placed at each end of the slit-pore. Placing the control volumes inside the pore eliminates pore-entrance effects and greatly simplifies the interpretation of our results. The volume of the control volumes is taken to be the same as that of the flow region in between them (see Fig. 1).

The control volumes and the flow region each have a length in the x-direction of $L_x = 13.3\sigma_f$, and a length in the y-direction of $L_y = 20.0\sigma_f$. We note that there is no unambiguous definition of volume in a porous membrane. However for simplicity, we define the volume of the flow region and control volumes to be $V = HL_xL_y$, which contains a certain amount of dead space due to the implicit carbon atoms in graphite. The pore widths studied were $H = 2.5\sigma_f$, $5.0\sigma_f$ and $10.0\sigma_f$.

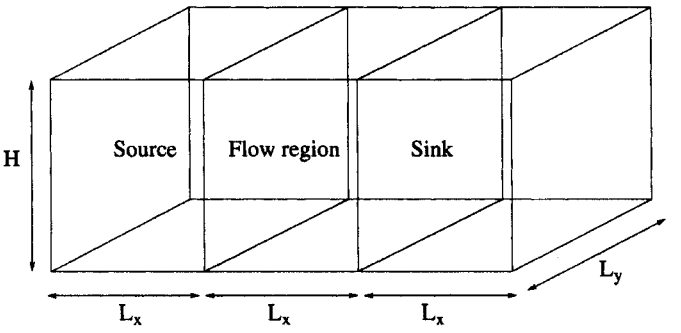

FIGURE 1 Schematic diagram of the simulation cell for DCV GCMD. Flow takes place in the x-direction from the source control volume to the sink control volume.

The DCV GCMD algorithm consists of performing numerous cycles, each of which comprises a molecular dynamics step, in which the trajectories of all fluid molecules are incremented, followed by a series of grand canonical Monte Carlo creations and destructions of methane molecules in each of the two control volumes.

A creation attempt of a methane molecule in control volume c is accepted with a probability,

$$\min[1, \exp[-\beta\Delta v + \ln(z(c)V(c)/(N+1))]] \tag{8}$$

where $V(c)$, N and $z(c)$ are the volume, the current number of molecules in control volume c and the methane activity in control volume c, respectively, while Δv is the energy change accompanying the insertion of a molecule into the control volume and $\beta = 1/k_B T$.

Destructions of molecules are accepted with a probability

$$\min[1, \exp[-\beta\Delta v + \ln(Nz(c)/V(c))]] \tag{9}$$

where Δv is now the energy change accompanying the destruction of a molecule from control volume c.

When molecules are created in either control volume, they are assigned thermal components of velocity selected from a Maxwell-Boltzmann distribution. Furthermore, newly created molecules are given an appropriate initial component of streaming velocity to ensure creations are compatible with mass transport (further details are given below).

The system is kept isothermal *via* the following scheme: The simulation box is divided into 21 bins of equal volume along the flow direction. The local temperature in each bin is then controlled by means of a Nosé-Hoover thermostat [16, 17].

The local temperature in each bin is defined by

$$\langle T(x_{\text{bin}})\rangle = \frac{\left\langle \sum_{i\in\text{bin}}^{N_{\text{bin}}} [\mathbf{p}_i - M_i\mathbf{u}(x_{\text{bin}})] \cdot [\mathbf{p}_i - m\mathbf{u}(x_{\text{bin}})] \right\rangle}{\langle 3N_{\text{bin}} - d(N_{\text{bin}}/N)\rangle} \tag{10}$$

where $\mathbf{u}(x_i)$ is the local average streaming velocity in bin i, N_{bin} is the number of molecules in a particular bin, N is the total number of molecules and d is the number of parameters that are used in the least squares fit of the molecular velocities to a given functional form. In this work we have fitted the streaming velocities to a two- parameter linear equation, and therefore, $d = 2$. The factor (N_{bin}/N) then accounts for the fraction of d alloted to each bin.

The presence of an adsorbent interaction field means that the streaming velocities will have a dependence on both the x and z-coordinates. However, for simplicity, we average over the z-coordinate, leaving only the x-dependence. Resolving the streaming velocity in the z-coordinate was found to make no difference to the calculated temperature profile or the diffusion coefficients [18].

To ensure that molecular creations are compatible with mass transport, a component of streaming velocity is added to the thermal velocity of newly created molecules. We determine this component of streaming velocity by taking a value for the flux at the center of the flow region and dividing this by the concentration in the appropriate control volume. Since we begin the simulation with zero molecules, initially there will be no measurable flux. As molecules begin to diffuse through the pore, a steady state flux will gradually develop, which is constant at any yz plane in the simulation cell. To prevent the streaming velocity from diverging, we follow Cracknell *et al.* [3] and introduce a degree of course graining. The method of augmenting the molecular velocities upon creation proceeds as follows: we allow a certain settling time, say 50000 steps, for obtaining sufficient molecules in the flow region to obtain a flux. After this time, we divide the flux (averaged over the settling time) by the average concentration of that species in the control volume of interest. The streaming velocity is then added to the thermal component of velocity of newly created molecules in that control volume. After the settling time, we average the flux over periods of 1000 molecular dynamics steps and use this value in the subsequent calculations of the streaming velocity in the end sections.

Because we employ a smooth potential to represent the graphite planes in a real carbon pore, we need to account for the exchange of momentum which would take place between fluid molecules and the carbon atoms in a real adsorbent. We employ the so-called diffuse boundary condition, based on the diffuse boundary conditions used by Cracknell *et al.* [3]. Application of the diffuse boundary condition proceeds as follows: After each molecular dynamics time step we check to see if the following two conditions are satisfied: (1) the momentum (in the laboratory frame) of a given molecule in the z-direction has reversed in sign; (2) the molecule is within the repulsive region of the Steele 10-4-3 potential. If, and only if, both of these conditions are satisfied, we reselect the momentum of that molecule in the directions parallel to the confining surface from a Maxwell-Boltzmann distribution at the appropriate temperature.

For the ratio of stochastic to dynamic steps, n_{MC}/n_{MD}, we chose a value of 120 for these simulations. In a molecular dynamics step, a fifth order Gear

algorithm [19] was used to integrate Hamilton's equations of motion, supplemented with a Nosé-Hoover thermostatting scheme [16, 17]. The integration time step was chosen to be 2.75 fs. Periodic boundary conditions operate in the y-direction. There are no periodic boundary conditions in the x-direction; the ends of the simulation box are dissolving boundaries. If a molecule reaches either of these boundaries it is removed from the simulation. The temperature employed in these simulations was: $T = 296.2\,\mathrm{K}$, while the source and sink control volume activities were: $z = 0.5424\,\mathrm{nm}^{-3}$ and $z = 0.3616\,\mathrm{nm}^{-3}$, respectively. We note that in real experiments, the control parameter would be the pressure rather than the activity. However, the activity can always be related to the pressure of the external bulk gas phase through an equation, of state and so comparisons could be made with experiment, provided one takes into account the distribution of slit widths (pore sizes) found in real microporous carbon samples.

4.3. Poiseuille Flow Algorithm

In the planar Poiseuille flow algorithm a constant force is applied to all fluid molecules directed along the x-axis (see for example Refs. [13, 14, 20] for further details on this method). Periodic boundary conditions operate in the x and y directions. The important point to note about this algorithm is that since an applied force drives the flow rather than a pressure gradient and the system is periodic in two dimensions, there are no density gradients along the flow direction (and hence no transport diffusion along that direction). Diffuse boundary conditions are employed to compensate for the lack of momentum exchange between a fluid molecule and the implicitly modelled graphite planes.

The Poiseuille flow simulations were conducted using the same model pore system employed in the DCV GCMD simulations. Simulations were conducted at the same three pore widths, and temperature. The pressure gradient is given by $dp/dx = \Delta p/L_x$ where Δp is the difference between the source and sink bulk external gas phase pressures. To determine the source and sink bulk gas pressures we conducted separate bulk grand canonical Monte Carlo simulations at the temperature and activities appropriate to the source and sink control volumes. These pressures are calculated to be: $p_{\mathrm{src}} = 2.3\,\mathrm{MPa}$ and $p_{\mathrm{snk}} = 1.5\,\mathrm{MPa}$. The external force needed in the simulations is calculated from the ratio of the pressure gradient to the mean DCV GCMD density. The number densities and external force magnitudes used in these simulations are given in Table I.

TABLE I Parameters used in the Poiseuille flow simulations

H/σ_f	N	ρ ($mmol\,cm^{-3}$)	$10^{14}F^{ext}$ (N)
2.5	1444	8.856	2.931
5.0	1352	5.510	4.712
10.0	1440	3.029	8.568

Starting configurations were obtained by simply placing the methane molecules on a lattice within the pore and equilibrating without the field for 2×10^6 steps and then equilibrating for a further 2×10^6 steps with the field switched on. Averages were then taken over production runs consisting of 20×10^6 steps. In order to obtain high signal to noise ratios, a large number of particles was chosen for these simulations. The values of N employed are given in Table I.

4.4. Equilibrium Simulations

Adsorption isotherms were obtained for the $H = 5.0\,\sigma_f$ and $H = 10.0\,\sigma_f$ case by conducting GCMC simulations [19, 21] within the pore. A range of fugacities was scanned and the density of molecules within the pore space was measured. For the $H = 2.5\,\sigma_f$ pore width, adsorption data were taken from the literature [9].

Equilibrium molecular dynamics simulations in the NVT ensemble were conducted for the purpose of calculating the self diffusivities and the mobility coefficients. The latter values were used as a verification of the subtraction method. Application of the Einstein relations involving mean squared displacements of the atomic positions and fluid center-of-mass position then gave the coefficients D_S and D_0. The length of these simulations varied from 12 million time steps for a typical estimate of the self diffusivity to 34 million time steps for an estimate of the mobility coefficient.

5. RESULTS AND DISCUSSION

5.1. DCV GCMD Simulations

The density of the pore fluid is plotted as a function of the scaled coordinate $2z/H$ in Figure 2. The profiles for the three pore widths are quite different. The narrow pore width profile displays two closely spaced prominent maxima. The widest pore profile also possesses two prominent maxima, but

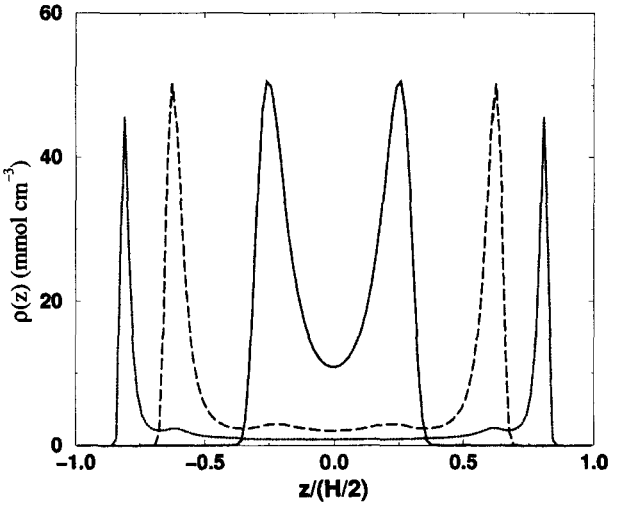

FIGURE 2 Concentration profiles along the z-direction for the 3 different pore widths studied: $H = 2.5\sigma_f$ (solid line), $H = 5.0\sigma_f$ (dashed line) and $H = 10.0\sigma_f$ (dotted line).

these are more widely spaced. Between the two adsorbed layers the fluid density is quite low but shows evidence of a weak layering effect. For $H = 5.0\sigma_f$, four fluid layers can be discerned, the innermost layers being weak in comparison to the outer ones. Figure 2 reveals the large changes in fluid packing which result from decreasing the pore width. Overlapping absorbent potential energy fields produce very deep energy wells leading to strong adsorption. As the pore width decreases the excluded volume of the implicit carbon atoms in the innermost graphite planes becomes a significant proportion of the total, physical pore volume.

A mean density was extracted from each of the DCV GCMD simulations by integrating the profiles in Figure 2 over the half interval [0, 1]. These densities, collected in Table II, show a trend of increasing density with decreasing pore width.

The density profiles measured along the flow direction for the three pore widths were found to show a linear variation with x in the flow regions, in agreement with Ficks law. Figure 3 shows the typical behaviour of the density in the $H = 5.0\sigma_f$ pore width simulation. Effective transport diffusivities were calculated from the ratio of the flux to the slope of the density in the flow region. These values are collected in Table II. While the total flux decreases with decreasing pore width, the effective transport diffusivities do not show this trend; the diffusivity at the lowest pore width is greater than that of the intermediate pore width.

TABLE II Results obtained from the DCV GCMD simulations. Numbers in parentheses are the statistical uncertainties in the last digit

H/σ_f	$\langle N \rangle$	J_x^{tot} $(mol\ cm^{-2}\ s^{-1})$	$d\rho/dx$ $(mol\ mm^{-4})$	$\langle \rho \rangle$ $(mmolcm^{-3})$	$10^3 D_t^{eff}$ $(cm^2 s^{-1})$
2.5	588	3.4(1)	−0.126(2)	8.856	2.67(8)
5.0	733	3.79(8)	−0.2659(3)	5.510	1.43(3)
10.0	805	4.08(8)	−0.1418(8)	3.029	2.87(5)

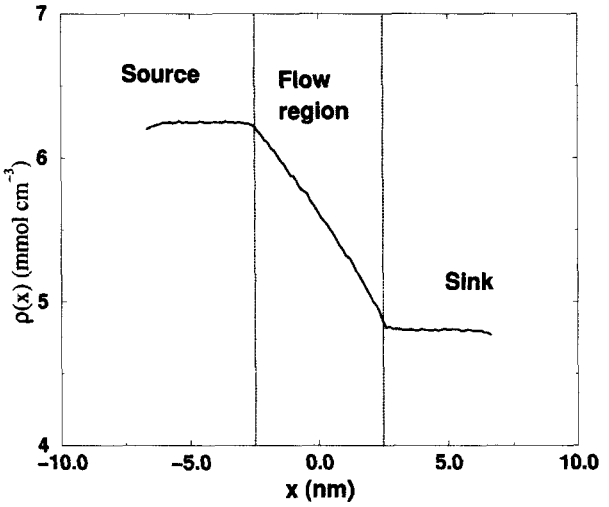

FIGURE 3 Concentration profile along the x-direction obtained from the $H = 5.0\sigma_f$ pore width simulation.

5.2. Poiseuille Flow Simulations

The transverse density profiles in the Poiseuille flow simulations were found to be identical to those from the DCV GCMD simulations indicating that for this pressure gradient, the nature of the flow has no significant effect on the fluid structure. Figure 4 shows the flux profiles plotted against the scaled z coordinate for the $H = 5.0\sigma_f$ simulation. The solid line represents the DCV GCMD flux while the dashed line represents the Poiseuille flow flux. The two profiles are qualitatively identical, differing only in their magnitude. The extra diffusive flux present in the DCV GCMD simulation gives rise to this difference. The average flux in the x direction in the Poiseuille flow simulations is obtained by first symmetrising, and then numerically integrating the flux profile in Figure 4 over the interval [0, 1]. Table III gives the average Poiseuille flux obtained from all three simulations. The values show

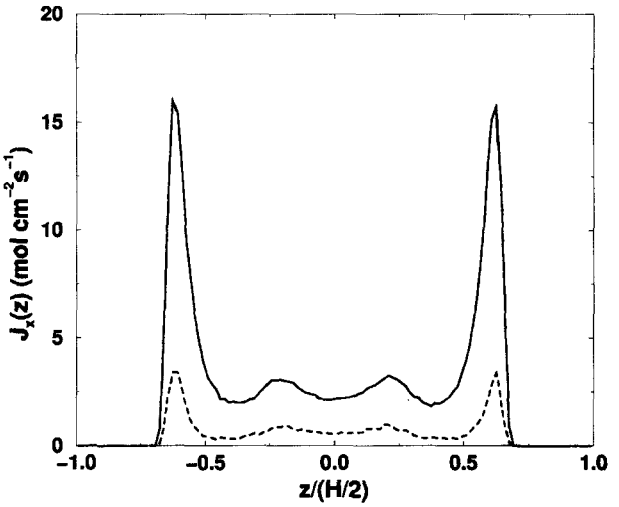

FIGURE 4 Flux profiles along the z-direction obtained from the DCV GCMD simulation (solid line) and the Poiseuille flow simulation (dashed line) with $H = 5.0\,\sigma_f$.

TABLE III Results obtained from the Poiseuille flow simulations

H/σ_f	$\langle J_x^V \rangle$ $(mol\ cm^{-2}s^{-1})$
2.5	0.3479
5.0	0.5701
10.0	1.373

a trend of decreasing flux with decreasing pore width though these decreases are much less than would be anticipated if Eq. (1) were true.

Figure 5 shows the velocity profiles obtained from the three Poiseuille flow simulations at different pore widths. These profiles were obtained by taking the ratio of the flux profiles to the density profiles. The velocity profiles have an underlying quadratic character in accordance with classical Navier-Stokes theory (the solid lines are the least squares fits of the data to a two parameter quadratic function). The Navier-Stokes equations are normally solved using no-slip (stick) boundary conditions which means that the velocity profiles can always be expressed in terms of a single adjustable parameter. From Figure 5 it is clear that the usual no-stick boundary conditions do not apply; the velocities do not extrapolate to zero at the physical boundaries. Koplik and Banavar [22] interpret this behaviour as microscopic slip. At the pore widths we have studied, the location of the "wall"s or boundaries cannot be expressed without ambiguity. The excluded

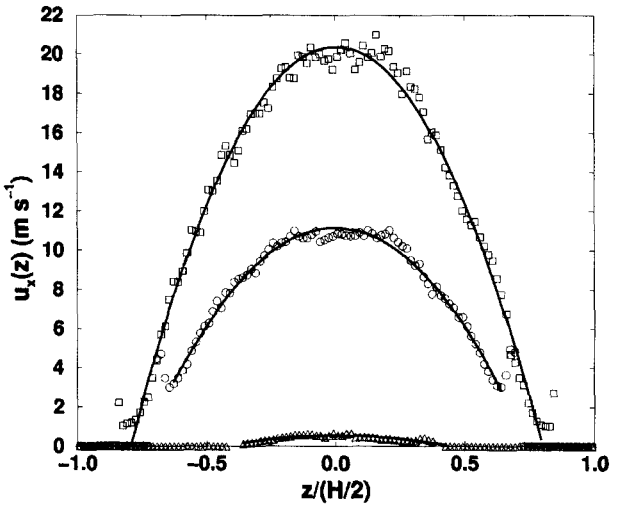

FIGURE 5 Velocity profiles along the z-direction obtained from the Poiseuille flow simulations for the 3 pore widths studied: $H = 2.5\sigma_f$ (triangles), $H = 5.0\sigma_f$ (circles) and $H = 10.0\sigma_f$ (squares). The solid lines are the least squares fits of the data to a 2 parameter quadratic function.

volume of implicit wall atoms becomes increasingly significant as the pore width decreases. If the location of the walls is taken to be the plane of closest approach to the carbon atoms in graphite then the velocity profiles appear to extrapolate to zero at this point (at least within the statistical uncertainties of our data). With this interpretation, our results could be taken to imply that slip does not occur. More precise data is needed to quantify this.

The velocity maxima in Figure 5 decrease with decreasing pore width. In the lowest pore width case, the velocity profile is very weak suggesting that in pores of this dimension, Poiseuille flow is negligibly small.

5.3. Darken Factors

Our measured isotherms were fitted to the following equation

$$\ln f = A + \ln \rho + B_1\rho + B_3\rho^3 + B_5\rho^5 \tag{11}$$

in which A, B_1, B_3 and B_5 are variable parameters. The Darken factor follows from Eq. (11) by differentiating with respect to $\ln \rho$

$$\frac{d \ln f}{d \ln \rho} = 1 + B_1\rho + 3B_3\rho^3 + 5B_5\rho^5 \tag{12}$$

Darken factors for all three pore widths are collected in Table IV. These Darken factors were evaluated using the mean densities obtained from the DCV GCMD simulations. The Darken factor for the narrowest pore width was evaluated using the data of Nicholson [9]. The Darken factor at the narrowest pore width is almost 4 times greater than the values of either of the other pore widths. The high value for the Darken factor in the narrow pore offsets the lower value of the mobility, with the result that the transport diffusivity is larger at the narrower pore width. Figure 6 shows a plot of the Darken factor as a function of concentration for the 3 pore widths studied (the data were generated using Eq. (12)). At low concentration, all three Darken factors approach unity as expected from a consideration of the zero concentration limit of Eq. (12). At higher concentrations the Darken factors show different qualitative behaviour. For the narrowest pore

TABLE IV Diffusion coefficients and Darken factors. Numbers in parentheses are the statistical uncertainties in the last digit

H/σ_f	$10^3 D_t$ ($cm^2 s^{-1}$)	$10^3 D_0$ ($cm^2 s^{-1}$)	$10^3 D_S$ ($cm^2 s^{-1}$)	$10^3 D_\xi$ ($cm^2 s^{-1}$)	$d\ln f/d\ln\rho$
2.5	2.4(1)	0.44(2)	0.137(1)	0.303(1)	5.50
5.0	1.21(3)	0.84(2)	0.4434(4)	0.40(1)	1.44
10.0	1.91(3)	1.40(2)	1.12(1)	0.28(1)	1.36

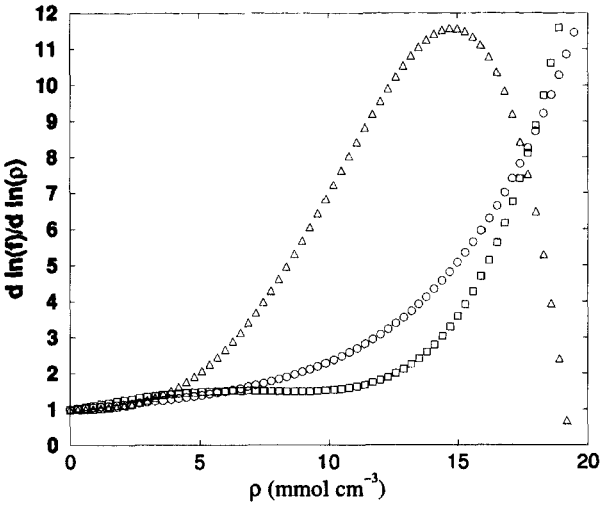

FIGURE 6 Darken factors ($d\ln(f)/d\ln(\rho)$) plotted as a function of concentration for the pore widths: $H = 2.5\,\sigma_f$ (triangles), $H = 5.0\,\sigma_f$ (circles) and $H = 10.0\,\sigma_f$ (squares). The Darken plot for $H = 2.5\,\sigma_f$ was generated from the data of Nicholson (Ref. [9]).

width, the Darken factor increases most rapidly, reaching a maximum at a concentration of 15 mmol cm^{-3}. At the widest pore width the Darken factor possesses a local maximum and a local minimum at concentrations of 5 mmol cm^{-3} and 10 mmol cm^{-3}, respectively. All three Darken factors have the same value at a concentration of approximately 17 mmol cm^{-3} , but then diverge from each other.

5.4. Diffusion Coefficients

The transport diffusivities were calculated by first subtracting out the Poiseuille contribution to the total DCV GCMD fluxes and then normalising by the concentration gradients. Mobility coefficients were obtained by dividing the transport diffusivities by the Darken factors, while D_ξ values were obtained from the mobilities by subtracting off the self diffusivity values. All the relevant diffusivities are collected in Table IV. Comparison of the transport diffusivities with the effective transport diffusivites in Table III demonstrates the difficulty involved in interpreting the latter values. The widest pore width has the largest effective transport diffusivity while it is the narrowest pore width which has the greatest transport diffusivity. The mobilities show a trend towards decreasing mobility with decreasing pore width. The Darken factors are responsible for the shift in relative values of the transport diffusivities, which means that the narrowest pore width can lead to the lowest mobility yet can also yield the highest transport diffusivity. Self diffusivities and the cross correlation diffusivities follow the same trend as the mobilities. Table V gives the weightings of each component of the flux (diffusive and viscous) as a percentage of the total DCV GCMD flux. The weightings of the self and cross correlation diffusivities as a percentage of the mobilities are also collected in the same table. Taking the fluxes first, we see a clear trend towards the decreasing role played by viscous flow as the pore width decreases. In the widest pore the viscous part of the total flux is 34% while in the lowest pore case, it is only 10%. Focusing on the diffusivity ratios, we see the increasing importance of the cross correlation term as pore width decreases. At the lowest pore width, the cross correlation diffusivity accounts for as much as 69% of the total

TABLE V Flux and diffusivity ratios

H/σ_f	J_x^V/J_x^{tot} (%)	J_x^D/J_x^{tot} (%)	D_S/D_0 (%)	D_ξ/D_0 (%)
2.5	10	90	31	69
5.0	15	85	53	47
10.0	34	66	80	20

mobility. These results show that gross errors would be incurred if transport diffusivities were calculated from the product of the self-diffusivity and the Darken factor, at least at the densities we have considered.

As a test of the subtraction method we calculated the transport diffusivities from the product of the Darken factors with directly calculated values of the mobility coefficients. As we discussed in the introduction, this route to the transport diffusivity is inferior to the present method since it is statistically inefficient. Nevertheless, it serves to verify the subtraction method. For the two lowest pore widths, we obtain mobility values of $D_0 = 0.46(3) \times 10^{-3}\,\mathrm{cm}^2\,\mathrm{s}^{-1}$ and $D_0 = 0.93(7) \times 10^{-3}\,\mathrm{cm}^2\,\mathrm{s}^{-1}$ respectively. These mobility values were obtained from equilibrium molecular dynamics simulations *via* integration of the streaming velocity autocorrelation function. Comparison with the mobilities calculated by subtraction shows that all values are in agreement within the statistical uncertainty of the data. We were unable to obtain a reasonably accurate value for the mobility coefficient *via* the equilibrium route at the widest pore width studied.

6. CONCLUSIONS

We have demonstrated a novel simulation method in which the separate contributions to the total flux can be determined. The method involves the use of two non-equilibrium molecular dynamics techniques: dual control volume grand canonical molecular dynamics (DCV GCMD) and an algorithm for simulating planar Poiseuille flow. The subtraction method is superior to the alternative route *via* direct calculation of D_0 for calculating the transport diffusivity. This alternative route relies upon correlating equilibrium fluctuations of the N particle property, the barycentric velocity, and so is statistically inefficient. We applied this technique to study the combined (viscous and diffusive) transport of methane through single slit-shaped graphite pores of width 2.5, 5.0 and 10.0 methane diameters. We find that the viscous contribution to the total intra-pore flux through each of these pores is 10%, 15% and 34%, respectively. The viscous contribution to the total flux does not scale as the square of the pore width, as a crude, Navier-Stokes analysis suggests it should. As the pore width decreases, the contributions to the mobility coefficient arising from momentum correlations between different adsorbate atoms dominates the contributions from self correlations.

The viscous subtraction method can readily be applied to the transport of mixtures in slit-pores. The role played by viscous flow in the transport and separation of binary mixtures is the subject of our future work.

Acknowledgments

The authors would like to thank Dr. David Nicholson and Professor Denis Evans for useful discussions during the course of this work. We are grateful to the National Science Foundation for the support of this work through research grant No. CTS-9896195; supercomputer time was provided through a NSF NPACI grant (No. NPA 205).

References

[1] Heffelfinger, G. and van Swol, F. (1994). "Diffusion in Lennard-Jones fluids using dual control volume grand canonical molecular dynamics simulation (DCV-GCMD)", *J. Chem. Phys.*, **100**, 7548.
[2] MacElroy, J. M. D. (1994). "Nonequilibrium molecular dynamics simulation of diffusion and flow in thin microporous membranes", *J. Chem. Phys.*, **101**, 5274.
[3] Cracknell, R. F., Nicholson, D. and Quirke, N. (1995). "Direct molecular dynamics simulation of flow down a chemical potential gradient in a slit-shaped micropore", *Phys. Rev. Lett.*, **74**, 2463.
[4] Pohl, P. I., Heffelfinger, G. S. and Smith, D. M. (1996). "Molecular dynamics computer simulation of gas permeation in thin silicalite membranes", *Mol. Phys.*, **89**, 1725.
[5] Ford, D. M. and Heffelfinger, G. S. (1998). "Massively parallel dual control volume grand canonical molecular dynamics with LADERA II. Gradient driven diffusion through polymers", *Mol. Phys.*, **94** , 673.
[6] MacElroy, J. M. D., Friedman, S. P. and Seaton, N. A. (1998). "On the origin of transport resistances within carbon molecular sieves", *Chem. Eng. Sci.*, submitted.
[7] Travis, K. P. and Gubbins, K. E. (1998). "Transport diffusion of a mixture of oxygen and nitrogen in a carbon slit *via* dual control volume grand canonical molecular dynamics (DCV GCMD)." In: Meunier, F., Ed., "*Fundamentals of Adsorption*", Volume 6, Elsevier, Paris.
[8] Travis, K. P. and Gubbins, K. E. (1999). "Transport diffusion of oxygen-nitrogen mixtures in graphite pores: a non-equilibrium molecular dynamics (NEMD) study", *Langmuir*, **15**, 6050.
[9] Nicholson, D. (1998). "Simulation studies of methane transport in model graphite micropores", *Carbon*, **36**, 1511.
[10] Mason, E. A. and Viehland, L. A. (1978). "Statistical mechanical theory of membrane transport for multicomponent systems: passive transport through open membranes", *J. Chem. Phys.*, **68**, 3562.
[11] Mason, E. A. and Malinauskas, A. P. (1983). "Gas transport in porous media: the dusty gas model." Elsevier, Amsterdam.
[12] Nicholson, D. (1997). "The transport of adsorbate mixtures in porous materials: basic equations for pores with simple geometry", *J. Membrane Sci.*, **129**, 209.
[13] Travis, K. P., Todd, B. D. and Evans, D. J. (1997). "Departure from Navier-Stokes hydrodynamics in confined liquids", *Phys. Rev. E*, **55**, 4288.
[14] Todd, B. D., Evans, D. J. and Daivis, P. J. (1995). "Pressure tensor for inhomogeneous fluids", *Phys. Rev. E*, **52**, 1627.
[15] Steele, W. A. (1974). "The interaction of gases with solid surfaces", Pergamon, Oxford.
[16] Nose, S. (1984). "A unified formulation of the constant temperature molecular dynamics method", *J. Chem. Phys.*, **81**, 511.
[17] Hoover, W. G. (1985). "Canonical dynamics – equilibrium phase-space distributions", *Phys. Rev. A*, **31**, 1695.
[18] Travis, K. P. and Gubbins, K. E., "Unpublished work".
[19] Allen, M. P. and Tildesley, D. J. (1987). "Computer simulation of liquids", Clarendon Press, Oxford.

[20] Travis, K. P. and Gubbins, K. E., "Poiseuille flow of WCA and Lennard-Jones fluids in narrow slit pores", *J. Chem. Phys.*, In press.
[21] Frenkel, D. and Smit, B. (1996). "Understanding molecular simulation". Academic Press, San Diego.
[22] Koplik, J. and Banavar, J. R. (1995). "Continuum deductions from molecular hydrodynamics", *Annu. Rev. Fluid Mech.*, **27**, 257.